Wear 498–499 (2022) 204284

Contents lists available at ScienceDirect

Wear

journal homepage: www.elsevier.com/locate/wear

# Measuring multi-asperity wear with nanoscale precision

Cyrian Leriche [a,b,*], Steve Franklin [a], Bart Weber [a,b]

[a] Advanced Research Center for Nanolithography (ARCNL), Science Park 106, 1098 XG, Amsterdam, the Netherlands
[b] Van der Waals-Zeeman Institute, Institute of Physics, University of Amsterdam, Science Park 904, 1098 XH, Amsterdam, the Netherlands

ARTICLE INFO

*Keywords:*
Wear detection
Multi-asperity
Pixel-level alignment
Asperity-scale wear
Topographical difference method

ABSTRACT

Wear of multi-asperity interfaces remains difficult to predict from first principles, in part because improvements are required in our ability to quantify and track wear across the micro-to nanometer scale. In this work, we developed a 6° of freedom topographical difference method based on large atomic force microscopy (AFM) measurements, up to 90 × 90 μm$^2$ in size. We detect wear volumes as small as $1.6 \times 10^{-11} \pm 3.7 \times 10^{-12}$ mm$^3$ (0.016 μm$^3$), beyond the sensitivity of many existing techniques for the quantification of wear at multi-asperity interfaces. We show that our wear detection technique can be combined with 100 mN normal force ball-on-flat friction experiments to track nanoscale wear across the entire area of apparent contact.

## 1. Introduction

Wear has a cost [1,2]: Industrialized nations have been estimated to spend more than 4% of their gross national product on replacing worn surfaces [3] such as tires, train rails or ceramic components made of silicon-based materials (cutting tools, MEMS/NEMS etc.). Despite its serious economic impact, the wear occurring at multi-asperity interfaces cannot be predicted accurately from first principles. Processes that may dominate wear at interfaces between silicon based materials include fatigue, fracture, abrasion and mechanochemistry. These wear processes are strongly influenced by the relative humidity, which sets the chemical landscape and the adhesion strength within the tribological system [4–11]. Especially in mild wear conditions, the nm length scale can play an important role in determining the wear behavior [12–14], yet it is difficult to measure wear at this scale for industrially relevant multi-asperity contacts.

High precision characterization of wear and contact mechanics is required to build a predictive understanding of wear at multi-asperity interfaces [15,16]. In addition, high precision wear measurements enable the bridging of concepts inspired by single-asperity experiments and simulations [17–19] to the realm of practical applications. Various precision wear detection techniques have been developed over the past 20 years [20–23]. High sensitivity wear detection for multi-asperity interfaces has been achieved through the use of optical profilometry: Burris et al. [24] detected wear volumes down to $2 \times 10^{-6}$ mm$^3$ using calibrated optical microscopy. Based on the same measurement technique, Garabedian et al. [25] used features of the surface that were not in contact as a reference to mechanically and computationally realign the pre-test and post-test images, enabling a wear sensitivity of $1 \times 10^{-10}$ mm$^3$. However, these optical profiling techniques have limited resolving power and can be influenced by changes in reflectivity of the surfaces.

Atomic force microscopy (AFM) methods can achieve higher spatial resolution and have also been used to map and quantify wear at sub-micron scales [26–28]. Gahlin et al. [26] developed an AFM topography difference technique to extract the local volume gained or lost during a scratch test. They used Nanoindentation marks to track surface locations before and after wear to detect wear volumes as small as $4 \times 10^{-8}$ mm$^3$. Furustig et al. [28] used the AFM image subtraction technique developed by Gahlin et al. [26] to quantify the wear of steel disks (flat-on-flat). In both studies [26,28] the use of indentation marks precludes the need for a post-test realignment procedure as the two images are realigned manually. Improvements beyond these previous studies are possible through increased AFM measurement resolution and optimized realignment. Furthermore, previous high resolution wear measurements have addressed the wear of the counter surface –not the slider– of the tribological system.

Here, we develop a method, based on the work of Gahlin et al. to overlap, realign and subtract AFM topography measurements of a multi-asperity surface with nanometer scale precision. A 6-degrees of freedom alignment procedure is applied to the AFM measurements recorded before and after wear in order to quantify the volume of material that has been gained and lost. Using a large sample AFM we scan sphere apex surfaces up to 90 μm in size with a spatial resolution better than 20 nm,

* Corresponding author. Advanced Research Center for Nanolithography (ARCNL), Science Park 106, 1098 XG, Amsterdam, the Netherlands.
*E-mail address:* c.leriche@arcnl.nl (C. Leriche).

https://doi.org/10.1016/j.wear.2022.204284
Received 16 November 2021; Received in revised form 31 January 2022; Accepted 10 February 2022
Available online 18 February 2022

enabling the quantification of wear from the nanoscale all the way up to the size of the apparent area of the sphere-on-flat contact. The presented wear detection method can be applied to both the slider and the counter-surface of the tribological system studied.

Our improved method enables the detection of wear volumes as small as $1.6 \times 10^{-11} \pm 3.7 \times 10^{-12}$ mm$^3$ at the asperity level ($800 \times 800$ nm$^2$), thereby providing new opportunities to connect fundamental insights in single asperity wear [17–20] to experiments with industrially relevant contact conditions.

## 2. Method and results

### 2.1. Samples

The surfaces used in this study were 3 mm diameter Silicon Nitride balls ($Si_3N_4$) polished to an ISOV* grade 5 (BC precision, root mean square height $h_{RMS\text{-}surface}$ = 15–20 nm as measured by AFM on a $30 \times 30$ μm$^2$ area). To investigate the effect of surface roughness on the wear detection method, some of the spheres were roughened to various degrees. Two methods were employed to achieve increased surface roughness. (i) The pristine sphere was placed in a plastic cylindrical tube (15 cm high, 3 cm diameter) together with a double-sided piece of sand paper ($3 \times 3$ cm$^2$, corundum particle size from 162 μm down to 8 μm) and the tube was subsequently inserted into a vortex shaker for 5–30 h of shaking at a frequency of 2000 rotations per minute. Collisions of the sphere onto the sand paper induced by the vortex shaker damage the sphere surface, thereby increasing the $h_{RMS\text{-}surface}$ up to 200 nm (measured by AFM on a $30 \times 30$ μm$^2$ area). (ii) Pristine spheres were subjected to a sand blasting procedure (0.8 μm particle size, 1, 2 and 3 bar of pressure for 5 s). The sand particles colliding with the sphere surface create sharp roughness peaks, resulting in an $h_{RMS\text{-}surface}$ roughness of up to 500 nm (measured by AFM on a $30 \times 30$ μm$^2$ area). Before AFM imaging, the spheres were cleaned through ultra-sonication in acetone, isopropanol and distilled water (PERMAK Compact 100, Best Water technology), each for 30 min.

### 2.2. Imaging technique

An AFM (Dimension ICON, Bruker) was used in tapping mode to collect $30 \times 30$ μm$^2$ measurements of the sphere apex topography (Fig. 1). Here, the AFM tip (RTESPA-300, Antimony (n) doped Si, Bruker) is oscillated in the normal direction at a predefined amplitude. Interaction between the tip and the sample results in a reduction in oscillation amplitude. A feedback loop between the measured tip oscillation amplitude and the z-position of the tip with respect to the surface enables the tip to scan the surface and map the local height changes. The measured topographs were processed using Gwyddion [29] software. Any measurement artifacts were corrected and a polynomial background was removed to flatten the topography. The roughness of each sample was extracted from these measurements and defined as the standard deviation from the mean height of the surface ($h_{RMS\text{-}surface}$).

### 2.3. Topographical difference method characterization with AFM setup

Three $Si_3N_4$ spheres, each with a different surface roughness, were used to characterize the quality of the topographical difference method presented. For each of these spheres, 5 subsequent $30 \times 30$ μm$^2$ AFM topography measurements (1024 lines, pixel size 29.3 nm) were performed. The samples were repositioned before each measurement. This procedure simulates the misalignment that occurs when the sphere was removed in between AFM measurements to perform a wear experiment. The sphere samples were clamped in a ball holder that was marked on one side such that the orientation of the sphere in the AFM system could be approximately matched. At the same time, the ball holder enabled placement of the spheres in various tribometers for sphere-on-flat friction and wear experiments. The main sources of mechanical misalignment are the stage repositioning accuracy (2 μm) and the sample orientation. We retrieved the approximate surface location by using the optical microscope equipped on the AFM to find the apex of the sphere. The positioning could be further optimized by making line scans with the AFM in two orthogonal directions and ensuring that the apex of the sphere was centered. A new tip was used for every topography measurement in order to limit the influence of tip wear. Difference maps from the alignment procedure were constructed by subtracting measurement 1 and 2, measurement 2 and 3, measurement 3 and 4 and, finally, measurement 4 and 5. We thus obtained 4 difference maps for each roughness.

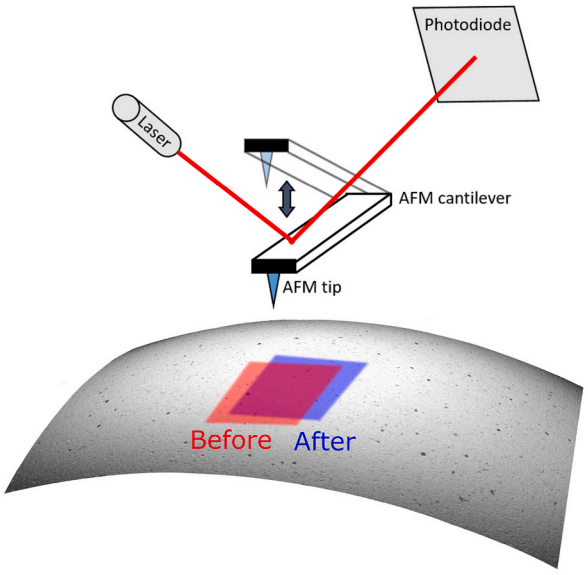


**Fig. 1.** Experimental setup. Subsequent images of a $Si_3N_4$ sphere surface, before and after a wear test, are taken using tapping mode AFM. The red and blue square illustrate the repositioning error caused by limited control over the placement of the sample in the AFM and over the AFM sample stage. (For interpretation of the references to colour in this figure legend, the reader is referred to the Web version of this article.)

### 2.4. Topographical difference method: alignment procedure

Matlab scripts were developed to align the topography measurements. To match the orientation of the topographies measured before and after repositioning (or wearing) the sample, we subjected the topographs to 6 realignment corrections, corresponding to the 6° of freedom illustrated in Fig. 2. The first step consisted of a rotational correction around the vertical axis (Yaw in Fig. 2). Next, lateral and longitudinal corrections were applied simultaneously. This was followed by a rotational correction around the lateral and longitudinal axis. Finally, the vertical offset between the two measurements was corrected. Each degree of freedom was optimized individually (except for the lateral and longitudinal corrections which were optimized simultaneously), while the other degrees of freedom were kept fixed. However, if necessary, the steps can be repeated once a first optimal value for all parameters has been obtained. The alignment is based only on the negative features of the pre and post test surfaces to ensure that we align unworn parts of the surface. Alignment based on all surface features can lead to non-negligible misalignment and thus inaccurate wear quantification (Supplementary Fig. 5).

In each correction step, we minimized the difference between the 'before' and 'after' topographies as a function of the displacement or rotation. The difference topography was defined as the 'after' topography minus the 'before' topography. Fig. 2 displays a typical outcome of the alignment procedure. The standard deviation of the pixel heights in this difference map quantifies the precision of the alignment

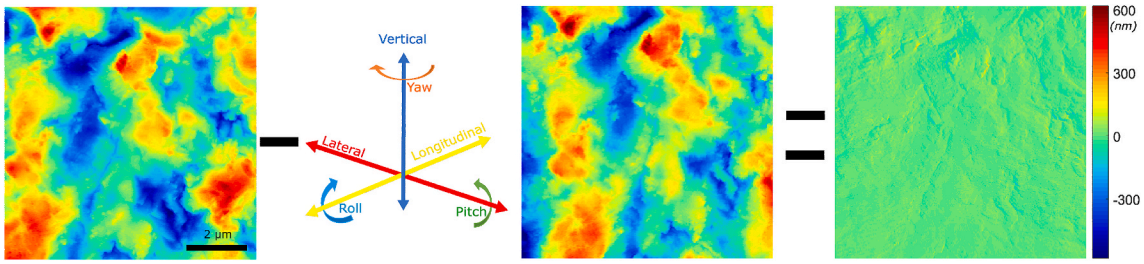


**Fig. 2.** Alignment procedure of the topographical difference method. The 'after' topography (center) was rotated and displaced in 6 different ways, as illustrated by the arrows, to give maximum resemblance to the 'before' topography (left). The actual resemblance was quantified by the difference map (right). All three maps were cropped from the original data.

procedure and the repeatability of the AFM measurement. We quantified the pixel height standard deviation across the full measured area using:

$$h_{RMS-diff} = \sqrt{\frac{\sum_{i=1}^{N}(x_i - \mu)^2}{N}} \quad (1)$$

Here, $x_i$ is the height of a single pixel of the map, N is the total number of pixels and μ is the mean value plan of heights across the map, which is 0 by definition. To disregard most of the false wear visible in the difference image we define a threshold:

$$T_{wear} = 2 \times h_{RMS-diff} \quad (2)$$

Pixels in the difference images only count toward the measured wear if the (absolute value of the) pixel height is larger than the threshold, $T_{wear}$. The height distribution of the control measurement (no wear) difference map (Supplementary Fig. 3) indicates that ~95% of the pixels in the difference map are within the $\pm 2 \times h_{RMS\text{-}diff}$ range, i.e. below the wear threshold $T_{wear}$. The total wear volume generated by the remaining 5% of pixels that do have heights that exceed the threshold is summed up to quantify the wear error ($V_{error}$) of the topographical difference method (corresponding to the full area to which the method is applied).

The values of the $Si_3N_4$ sample surface roughness, the standard deviation in heights ($h_{RMS\text{-}diff}$) in the difference images (see Supplementary Fig. 1 and Fig. 2) and the wear error are reported in Table 1. We confirmed that $h_{RMS\text{-}diff}$ depends only weakly on the image size. The wear detection depends more strongly on the surface roughness because the AFM imaging is more repeatable on smooth surfaces. Higher roughness means that the AFM tip needs to accurately follow more surface features during scanning. Sharp features on the surface require strong feedback parameters during AFM scanning which in turn increases measurement noise. A series of measurements have been performed on the rough sample, without repositioning (Supplementary Fig. 4) emphasizing that repositioning is not the main source of the wear error.

Wear that results from local height changes larger than $2 \times h_{RMS\text{-}diff}$, leading to an overall wear volume ($V_{wear}$) significantly larger than the wear error, can be reliably detected. In comparison to optical approaches to wear detection [24,25], the main advantage of the AFM based method presented here is the improved lateral resolution.

**Table 1**
Left column: Root mean square height of the sample surfaces measured by AFM on a $30 \times 30$ μm$^2$ area. Center column: Standard deviation of the difference map after the alignment procedure. 5 independent difference maps were analyzed. Right column: error on measured wear volume $V_{error}$; the wear volume detected after applying the wear threshold to the control experiment.

| $h_{RMS-surface}$ (nm) | $h_{RMS-diff}$ (nm) | $V_{error}$ (mm$^3$) for 23 × 23 μm$^2$ area |
|---|---|---|
| 16 | 1.8 ± 0.2 | $3.9 \times 10^{-11}$ |
| 173 | 2.5 ± 0.4 | $1.1 \times 10^{-10}$ |
| 264 | 16 ± 2.5 | $4.4 \times 10^{-10}$ |

### 2.5. Detecting nanoscale wear

Wear experiments were carried out using the $h_{RMS\text{-}surface} = 16$ nm $Si_3N_4$ sphere sliding against a silicon wafer. The sphere holder was loaded into a Universal Mechanical Tester (UMT Tribolab, Bruker) and brought into contact with a silicon wafer (100 mm diameter, University wafer, (100) crystal orientation, native oxide, $h_{RMS\text{-}surface} = 1$ nm as measured on a $5 \times 5$ μm$^2$ area) at a normal force of 100 mN. Subsequently a unidirectional, lateral displacement of 10 μm was imposed. This sliding cycle was repeated 2000 times in a non-repeated fashion [30]; each stroke was performed on a previously untouched part of the wafer by lifting the ball and displacing it laterally in between cycles. In this experiment, most of the displacement imposed on the sphere results in elastic deformation of the measurement system, rather than slip at the sphere-on-flat interface. The surface topography of the $Si_3N_4$ sphere was imaged in the AFM before and after the wear experiment and the topographical difference method was applied to the AFM topographs as described above. To ensure that the surface area that is scanned in the AFM has been (or will be) in contact with the counter surface during the wear experiment, AFM measurement areas were chosen so as to be larger than the calculated contact size. For a 3 mm diameter $Si_3N_4$ ball loaded with 0.1 N onto a flat silicon wafer, the Hertzian contact radius is 13.5 μm, which easily fits into the scan range of the AFM ($90 \times 90$ μm$^2$). Through the topographical difference method we could isolate different asperities (Fig. 3 and Supplementary Fig. 6) to detect asperity scale wear volumes as small as $1.6 \times 10^{-11} \pm 3.7 \times 10^{-12}$ mm$^3$ (0.016 μm$^3$). To define the asperity scale error in wear volume, we applied our wear criterion to an area of equal size on the corresponding control measurement in which no wear occurred. To obtain a conservative error estimate, we chose to select a region on the difference map within which the height variations were maximal.

## 3. Discussion

The topographical difference method [25,26,28] is conceptually simple yet not widely applied because without high precision repositioning and realignment of the topographs measured before and after wear, the resulting wear measurement is dominated by artifacts rather than actual wear. We presented a 6-degrees of freedom realignment method to correct the mechanical repositioning errors induced by mounting and unmounting the sample before and after wear experiments. Our post test realignment enables the detection of wear volumes significantly larger than $3.9 \times 10^{-11}$ mm$^3$ over an area of $23 \times 23$ μm$^2$ which corresponds to an average height change of 1.8 nm (Supplementary Fig. 1). While similar sensitivities in detecting height changes have been achieved through the topographical difference method applied to optical profilometry measurements, an advantage of the present method is the increased in-plane resolution offered by AFM. We detected asperity scale wear volumes as small as $1.6 \times 10^{-11} \pm 3.7 \times 10^{-12}$ mm$^3$ (0.016 μm$^3$). The main source of error in the wear detection originates from the repeatability of the AFM topography measurement, which scales with the roughness of the sample.

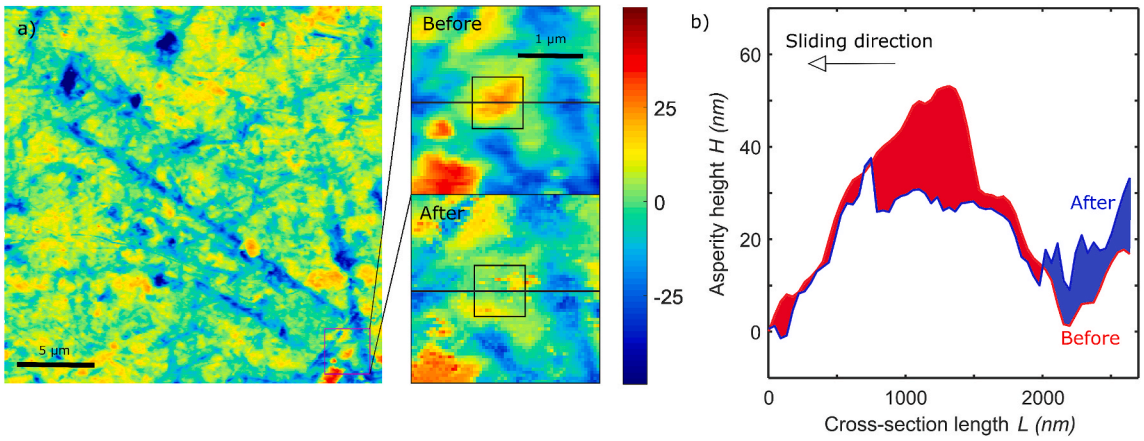


**Fig. 3.** Nanoscale wear of a multi-asperity interface. a) AFM measurement of a smooth Silicon Nitride sphere ($25 \times 25$ μm$^2$, $h_{RMS\text{-}surface} = 16$ nm). The zoom in shows topographs recorded before and after wear of the surface and focus on a single asperity that was worn off during the sliding against a silicon wafer. The wear volume associated with the asperity in the square is $1.6 \times 10^{-11} \pm 3.7 \times 10^{-12}$ mm$^3$ (0.016 μm$^3$). b) Lateral cross section of the isolated asperity before and after wear.

The developed 6° of freedom topographical difference method can easily be applied to study the evolution of the topography of slider and counter surface in a wide variety of tribological systems using any profilometer. Our results demonstrate that the limitation in the accuracy of the wear detection originates from the repeatability of the measurement device, not from the posttest realignment script (Supplementary Fig. 4).

## 4. Conclusion

We have presented a method to track and image sphere surfaces before and after wear against a counter surface using a combination of optical and atomic force microscopy. The AFM topographs recorded before and after wear were aligned and subtracted using a 6° of freedom computer script. We characterized the accuracy of the topographical difference method by applying the method to unworn surfaces. The detection of asperity scale wear volumes as small as $1.6 \times 10^{-11} \pm 3.7 \times 10^{-12}$ mm$^3$ was demonstrated. High accuracy wear detection, in combination with the topographical information of the full apparent area of contact opens up new possibilities for the study of wear and plasticity in relation to contact mechanics [31,32]. Our wear detection method can help bridge observations and insights made at a fundamental level in single asperity experiments and simulations to the multi-asperity interfaces that control applications in which friction and wear play a crucial role.

## Authorship agreement

The contribution to this work is divided among the three authors as follows:

- Cyrian Leriche: data curation, formal analysis, investigation, methodology, software, visualization, first role in writing.
- Steve Franklin: funding acquisition, project administration, resources, validation.
- Bart Weber: funding acquisition, investigation, project administration, supervision, 2nd role in writing.

## Data availability

All data used for this work and their corresponding scripts to generate the figure displayed are freely available on those two URLS: Generic alignment script (1) https://github.com/Cyrian-24/Measuring-multi-asperity-wear-with-nanoscale-precision–replication-package-scripts/Data of replication package (2) https://zenodo.org/record/6347044#.YitZ5ZYo9EY.

## Declaration of competing interest

The authors declare the following financial interests/personal relationships which may be considered as potential competing interests: Bart Weber reports financial support was provided by Dutch Research Council Domain Science.

## Acknowledgements

We thank Felix Cassin for sharing his ideas to understand and interpret the results shown in this work. A special thanks is also brought to Junxiao Du and Paul Ducarme for their help to make the alignment script versatile and usable by the most. We thank Feng-Chun Hsia for making two of the used samples for this study.

## Appendix A. Supplementary data

Supplementary data to this article can be found online at https://doi.org/10.1016/j.wear.2022.204284.

## References

[1] K. Holmberg, A. Erdemir, Influence of tribology on global energy consumption, costs and emissions, Friction 5 (3) (2017) 263–284, https://doi.org/10.1007/s40544-017-0183-5.
[2] K. Holmberg, A. Erdemir, Global impact of friction on energy consumption, economy and environment, FME Trans 43 (3) (2015) 181–185, https://doi.org/10.5937/fmet1503181H.
[3] E.H. Early, T. Jost, Lubrication (Tribology): Education and Research; a Report on the Present Position and Industry's Needs, H.M.S.O, London, 1996.
[4] J. Xu, K. Kato, Formation of tribochemical layer of ceramics sliding in water and its role for low friction, Wear 245 (1–2) (2000) 61–75, https://doi.org/10.1016/S0043-1648(00)00466-X.
[5] T.E. Fischer, H. Tomozawa, Interaction of tribochemistry and microfracture in the friction and wear of silicon nitride, Wear 105 (1985) 29–45.
[6] M.C. Mate, R.W. Carpick, Tribology on the Small Scale - A Modern Textbook on Friction, Lubrication, and Wear, Oxford graduate texts, 2019, p. 59.
[7] S. Jahanmir, Water lubrication of silicon nitride in sliding, Tribol. Lett. 40 (2) (2004) 50–62, https://doi.org/10.1023/B.
[8] Y. Qi, et al., Investigation of silicon wear against non-porous and micro-porous SiO2 spheres in water and in humid air, RSC Adv. 6 (92) (2016) 89627–89634, https://doi.org/10.1039/c6ra18152j.
[9] X. Dong, S. Jahanmir, Wear transition diagram of silicon nitride, Wear 5 (1993) 169–180, https://doi.org/10.1016/0043-1648(93)90332-G.
[10] W. Qin, W. Yue, C. Wang, Controllable wear behaviors of silicon nitride sliding against sintered polycrystalline diamond via altering humidity, Int. J. Lab. Hematol. 38 (1) (2018) 42–49, https://doi.org/10.1111/ijlh.12426.
[11] P. Xu, Y. Wang, X. Cao, X. Nie, W. Yue, G. Zhang, The tribological properties of DLC/SiC and DLC/Si3N4 under different relative humidity: the transition from abrasive wear to tribo-chemical reaction, Ceram. Int. 47 (3) (2021) 3901–3910, https://doi.org/10.1016/j.ceramint.2020.09.252.

[12] R. Colaço, A.P. Serro, Nanoscale wear of hard materials: an overview, Curr. Opin. Colloid Interface Sci. 47 (2020) 118–125, https://doi.org/10.1016/j.cocis.2020.01.001.
[13] C. Xiao, C. Chen, J. Guo, P. Zhang, L. Chen, L. Qian, Threshold contact pressure for the material removal on monocrystalline silicon by SiO2 microsphere, Wear 376–377 (2017) 188–193, https://doi.org/10.1016/j.wear.2016.11.028.
[14] J. Guo, et al., Interplay between counter-surface chemistry and mechanical activation in mechanochemical removal of N-faced GaN surface in humid ambient, Tribol. Int. 159 (January) (2021) 107004, https://doi.org/10.1016/j.triboint.2021.107004.
[15] V.L. Popov, R. Pohrt, Adhesive wear and particle emission: numerical approach based on asperity-free formulation of Rabinowicz criterion, Friction 6 (3) (2018) 260–273, https://doi.org/10.1007/s40544-018-0236-4.
[16] R. Aghababaei, D.H. Warner, J.F. Molinari, Critical length scale controls adhesive wear mechanisms, Nat. Commun. 7 (May) (2016) 1–8, https://doi.org/10.1038/ncomms11816.
[17] H. Bhaskaran, et al., Ultralow nanoscale wear through atom-by-atom attrition in silicon-containing diamond-like carbon, Nat. Nanotechnol. 5 (3) (2010) 181–185, https://doi.org/10.1038/nnano.2010.3.
[18] J. Liu, J.K. Notbohm, R.W. Carpick, K.T. Turner, Method for characterizing nanoscale wear of atomic force microscope tips, ACS Nano 4 (7) (2010) 3763–3772, https://doi.org/10.1021/nn100246g.
[19] T.D.B. Jacobs, R.W. Carpick, Nanoscale wear as a stress-assisted chemical reaction, Nat. Nanotechnol. 8 (2) (2013) 108–112, https://doi.org/10.1038/nnano.2012.255.
[20] D.L. Burris, W.G. Sawyer, A low friction and ultra low wear rate PEEK/PTFE composite, Wear 261 (3–4) (2006) 410–418, https://doi.org/10.1016/j.wear.2005.12.016.
[21] M. Scherge, The running-in of lubricated metal-metal contacts-a review on ultra-low wear systems, Lubricants 6 (2) (2018), https://doi.org/10.3390/LUBRICANTS6020054.
[22] M. Scherge, K. Pöhlmann, A. Gervé, Wear measurement using radionuclide-technique (RNT), Wear 254 (9) (2003) 801–817, https://doi.org/10.1016/S0043-1648(03)00230-8.
[23] R. Novak, T. Polcar, Tribological analysis of thin films by pin-on-disc: evaluation of friction and wear measurement uncertainty, Tribol. Int. 74 (2014) 154–163, https://doi.org/10.1016/j.triboint.2014.02.011.
[24] D.L. Burris, W.G. Sawyer, Measurement uncertainties in wear rates, Tribol. Lett. 36 (1) (2009) 81–87, https://doi.org/10.1007/s11249-009-9477-8.
[25] N.T. Garabedian, et al., Quantifying, locating, and following asperity-scale wear processes within multiasperity contacts, Tribol. Lett. 67 (3) (2019) 1–10, https://doi.org/10.1007/s11249-019-1203-6.
[26] R. Gahlin, A novel method to map and quantify wear on a micro-scale, Wear (1998) 93–102, https://doi.org/10.1016/S0043-1648(98)00287-7.
[27] H. Bosse, H. Kunzmann, G. Dai, F. Pohlenz, CIRP Annals - Manufacturing Technology Quantitative Analysis of Nano-Wear on DLC Coatings by AFM, vol. 62, 2013, pp. 543–546.
[28] J. Furustig, I. Dobryden, A. Almqvist, N. Almqvist, R. Larsson, The Measurement of Wear Using AFM and Wear Interpretation Using a Contact Mechanics Coupled Wear Model, vol. 351, 2016, pp. 74–81, https://doi.org/10.1016/j.wear.2016.01.002.
[29] Gwyddion : an open-source software for SPM data analysis, Cent. Eur. J. Phys. 10 (1) (2012), https://doi.org/10.2478/s11534-011-0096-2.
[30] F. Hsia, F.M. Elam, D. Bonn, B. Weber, S.E. Franklin, Wear particle dynamics drive the difference between repeated and non- repeated reciprocated sliding, Tribol. Int. 142 (October) (2019) 105983, https://doi.org/10.1016/j.triboint.2019.105983.
[31] T. Suhina, et al., Fluorescence microscopy visualization of contacts between objects, Angew. Chem. (2015) 3759–3762, https://doi.org/10.1002/ange.201410240.
[32] P. Audebert, D. Bonn, D. Petrova, B. Weber, A.M. Brouwer, Fast 3D microscopy imaging of contacts between surfaces using a fluorescent liquid, Appl. Mater. Interfac. (2018), https://doi.org/10.1021/acsami.8b15660.